Bulletin of Electrical Engineering and Informatics
Vol. 14, No. 1, February 2025, pp. 83~95
ISSN: 2302-9285, DOI: 10.11591/eei.v14i1.8548

Optimal deployment of solar PV power plants as fast frequency response source for a frequency secure low inertia power grid

Brian K. Wamukoya[1], Keren K. Kaberere[1], Christopher M. Muriithi[2]
[1]Department of Electrical and Electronic Engineering, College of Engineering and Technology, Jomo Kenyatta University of Agriculture and Technology (JKUAT), Nairobi, Kenya
[2]Department of Electrical and Electronic Engineering, School of Engineering and Technology, Murang'a University of Technology (MUT), Murang'a, Kenya

Article Info

Article history:

Received Apr 2, 2024
Revised Oct 4, 2024
Accepted Oct 17, 2024

Keywords:

Converter interfaced variable renewable energy sources
Deloaded mode
Fast frequency response
Low inertia
Particle swarm optimization
Solar photovoltaic power plant

ABSTRACT

Modern power systems are witnessing increased uptake of solar photovoltaic power plants (SPVPPs) replacing conventional synchronous generators (SGs). SPVPPs lack any rotating parts resulting in no natural rotational inertia contribution to the grid. Reduced inertia makes the power system more dynamic, making it susceptible to frequency instability caused by minor disturbances. This problem is majorly addressed by limiting the penetration of SPVPPs to ensure a minimum level of critical inertia is maintained or by providing additional virtual inertia from an energy storage system. However, the SPVPPs can be configured to operate below maximum power point tracking (MPPT) (deloaded mode) to provide a reserve capacity that can rapidly be deployed as fast frequency response (FFR) in case of a frequency event. This paper presents a strategy to optimize the FFR capacity of a deloaded SPVPP using particle swarm optimization (PSO) algorithm. DIgSILENT PowerFactory was used to model the deloaded SPVPP and run time domain simulations. PSO algorithm was implemented using a Python script in PowerFactory. The proposed strategy was applied on a modified IEEE 39 bus test system. The results show that optimal deloading of SPVPP can help to successfully arrest frequency decline, reduce power curtailment while adhering to the prescribed constraints.

Corresponding Author:

Brian K. Wamukoya
Department of Electrical and Electronic Engineering, College of Engineering and Technology
Jomo Kenyatta University of Agriculture and Technology (JKUAT)
Nairobi, Kenya
Email: wamukoya.brian@students.jkuat.ac.ke

1. INTRODUCTION

In the wake of escalating adverse impacts of climate change due to greenhouse gas (GHG) emissions and volatility in price and supply of fossil fuel sources like oil and gas globally, power grids across the globe have witnessed an unparalleled integration of converter interfaced variable renewable energy sources (VRES) like wind and solar in recent times. For the year 2020 alone, 238 GW of new installations of both solar (127 GW) and wind (111 GW) sources were integrated to different grids globally. Moreover, wind and solar sources accounted for about half of the total installed capacity of renewable energy sources worldwide [1]. It is expected that wind and solar will play a pivotal role in steering the energy transition for future power grids.

Solar photovoltaic power plants (SPVPPs) are connected to the power grid via power electronic converters which decouples them, meaning they are non-synchronously connected [2], [3]. SPVPPs are

considered inertia-less as they lack any rotating parts that can contribute to grid inertia [4]. Thus, replacing conventional fossil fuel fired plants with synchronous generators (SG) with SPVPPs reduces the effective grid inertia [5]. Grid inertia permits the power system to resist excursions in system frequency by using rotating masses of SGs [6]. Grid inertia is determined by the quantity of kinetic energy stored in rotating masses of SGs connected to the system. The kinetic energy stored in large rotating masses of SGs is released or absorbed (inertial response) naturally devoid of any control action during a power imbalance to slow down the rate of change of frequency (RoCoF). Grid inertia provides power to the grid extremely quickly before the active power management action of SGs (governor control) boosts active power output [7].

A grid with reduced inertia makes the power system more dynamic, which compromises frequency stability, resulting in a faster RoCoF, a significantly lower frequency nadir, and larger steady state frequency deviation even for minor power imbalances. Additionally, reduction in grid inertia reduces the time available to respond to a power imbalance [3], [8], [9]. Hence, concerns about the effects of lower inertia due to SPVPPs integration becomes a barrier to significantly increasing the plants installed capacity.

As power networks increase the share of SPVPPs installed capacity, it is critical that researchers investigate SPVPP's potential to provide supplementary energy balance services in the short term, to improve frequency control in inertia-deficient grids. Since decreased inertia reduces the time available to respond to power deficit, a fast-acting active power injection source is required. Ordinarily, SPVPPs are operated at maximum power point (MPP) to maximumly utilize the power available. To achieve the fast response, SPVPPs can be operated away from their MPP, known as deloaded mode, to have a reserve margin that can rapidly be deployed in case of a frequency event [10]. Such fast frequency response (FFR) from a SPVPP without turbine delay exploits the agility of power electronic converters and can be used as a short-term replacement of grid inertia for low inertia power grids. Even though some cheap source of power from the SPVPP is curtailed, the objective is to address frequency stability issues. FFR is considered slightly slower (due to latencies in measuring instruments) than inertial response from SGs but significantly faster that the primary frequency response (governor action) from SGs. The FFR mechanism rapidly injects active power into the grid proportional to the frequency deviation and the RoCoF hence, reducing overreliance on inertia from SGs for frequency regulation [11], [12]. The FFR intervention can be considered superior to SG inertia since it reduces RoCoF as well as improves frequency quality as opposed to inertia which only reduces RoCoF in case of a frequency event.

In literature, several proposals have been put across to address the low inertia problem. Majority of the sources reviewed focused on increasing levels of inertia (virtual inertia) using various energy storage technologies. The authors of [13]-[15] investigated the viability of deploying battery energy storage system (BESS) as a virtual inertia source. Research by Magdy *et al.* [13], a virtual SG was modelled based on superconducting magnetic energy storage which technically outperformed BESS-based virtual SG in frequency control in power grids with high penetration of SPVPP. A techno-economic assessment of deploying a wind power plant as a virtual inertia source was investigated in [16] and found it was viable for power grids with relaxed frequency stability indices. A sophisticated control strategy for harvesting the hidden inertia from wind turbines is presented in [17]. A techno-economic analysis of FFR provision from SPVPP versus BESS in carried out in [18]. BESS was found to be more effective providing frequency support than deloaded SPVPP though costlier. FFR provision from hybrid energy storage system including use of large capacitors was investigated in [19]. Performance distinction between FFR and virtual inertia contribution in frequency regulation was demonstrated in [20]. The performance of deploying SPVPPs as FFR sources was investigated in [11], [12], [21] and found to be technically viable. A detailed and comprehensive review of existing frequency control strategies in low inertia power grids can be found in [1], [22].

From the reviewed literature, there is very limited work done on optimization of SPVPP deloading level using metaheuristic approach. In addition, ecological emissions have not been considered in formulation of the optimization problem despite humanity being confronted by the climate change crisis. Much of this work is inspired by the work carried out in [11], [12], [23]. In literature, the performance of a deloaded SPVPP providing frequency support is only observed without giving proper justification or interpretation of the results. This paper serves to quantify the performance of fast frequency support from SPVPPs and deduce ideal FFR properties for better frequency support. In addition to considering power system operation costs, the work reported in this paper incorporates ecological emissions into the fitness function used to determine the optimal fast frequency reserve capacity using the particle swarm optimization (PSO) algorithm.

The major contributions of this paper include the following:

– Formulation of a techno-economic and environmental multi-objective optimization problem to determine the optimal deloading level of SPVPPs using PSO in DIgSILENT PowerFactory platform.

– Quantifying performance of deloaded SPVPP in frequency support and deducing the ideal properties of FFR support from deloaded SPVPPs.

The rest of this paper is organized as follows: section 2 highlights the modelling of a dynamic SPVPP and formulation of a multi-objective optimization problem. Section 3 presents the simulation setup and results. Discussion of results is done here as well. Finally, the conclusion and proposed areas of further research are presented in section 4.

2. METHOD

2.1. Dynamic modelling of a deloaded solar photovoltaic power plant

Power system operators conventionally operate SPVPPs in maximum power point tracking (MPPT) mode to draw maximum power available hence, no reserve is held. SPVPPs have in recent years been deployed for over-frequency control due to their ability to rapidly recede output power (curtailment) leveraging on the agility of power electronic converters, to prevent over-frequency generator tripping [24]. Alternatively, SPVPP can be operated away from their optimal operating point thus, creating a reserve margin that can quickly be deployed with the aid of appropriate supplemental control loops to support system frequency almost like conventional SGs. This is known as deloaded mode. The SPVPP in this mode acts as a source of FFR due to its ability to surge active power instantly to the grid in response to a frequency event [23].

Modelling of the dynamic SPVPP operating in deloaded mode was done in DIgSILENT PowerFactory environment as well as conducting time domain simulations to test the validity of the model. Deloading a SPVPP requires a modification in the control strategy of the converter. The converter is made to operate away from the maximum power point voltage - V_{mpp} which generates maximum power- P_{mpp} as shown in Figure 1. The choice of the operating voltage of the SPVPP on the DC side determines the output power. In the interest of guaranteeing stability, the converter on the DC side is operated at a voltage greater than V_{mpp} which is V_{red} or $V_{mpp} + V_{deload}$ generating a lower power output P_{red}. This modification results in the creation of a power reserve margin- $P_{deloaded}$ by the SPVPP which is given by (1):

$$P_{deloaded} = P_{mpp} - P_{red} \tag{1}$$

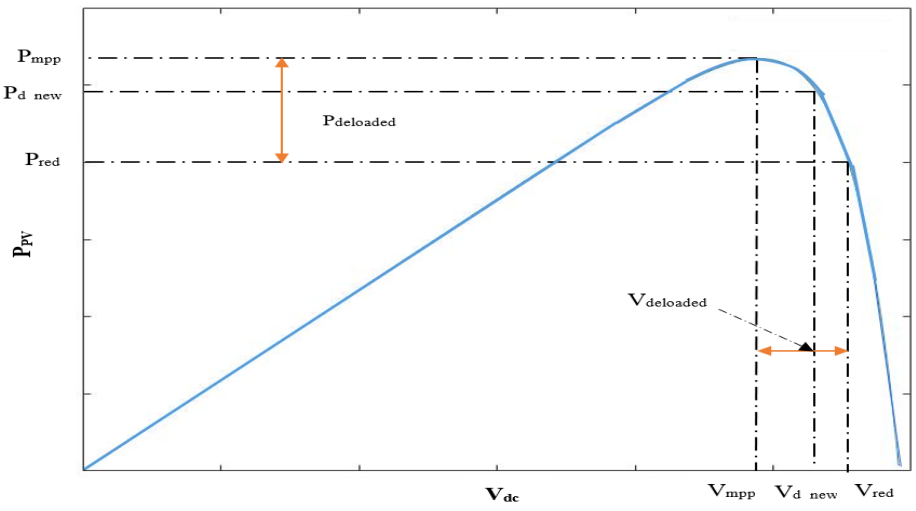

Figure 1. Deloaded SPVPP operation

To dispense the reserved power ($P_{deloaded}$) at a time of need, for instance, in the event of a contingency, a signal proportional to the frequency deviation (Δf) is subtracted from the DC output voltage of the SPV array (V_{red}) ramping up the active power delivered to a new power output- P_{d_new}. The active power controller realizing this strategy was implemented using DIgSILENT simulation language (DSL) and is shown in Figure 2. The new operating voltage point- V_{d_new} is given by (2) [25].

$$V_{d\_new} = V_{red} - K_g \Delta f = V_{mpp} + V_{deload} - K_g \Delta f \tag{2}$$

where K_g represents the proportional gain constant.

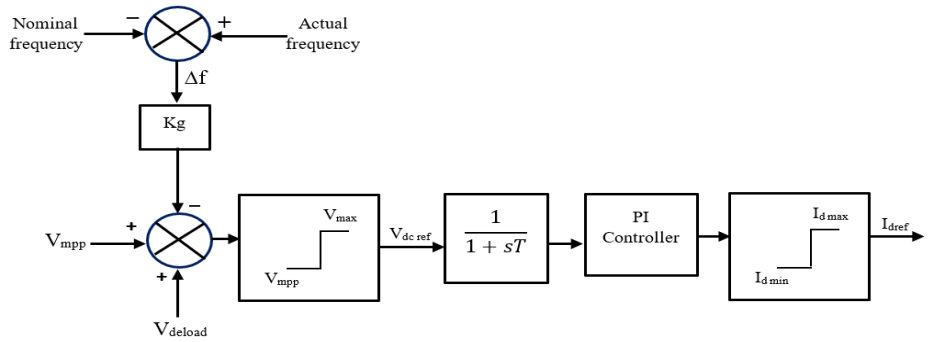

Figure 2. Active power controller for a deloaded SPVPP

A decline in system frequency because of a power imbalance causes the converter operating voltage V_{red} to decrease towards V_{mpp} thereby rapidly increasing active power output of the SPVPP (with possibility to reach P_{mpp}) to respond to the frequency disturbance. In this scenario, the SPVPP almost emulates the SG's primary frequency response without turbine delay. The active power controller implementing the frequency droop control is shown in Figure 2 [25].

2.2. Optimization problem formulation

A multi-objective (MO) optimization problem was formulated to minimize the aggregate power system generation cost and ecological emissions cost in a SPV penetrated grid. In general, a MO optimization problem takes the form (3):

$$Minimize, F(x,u) = [F_1(x,u), F_2(x,u) \ldots . F_i(x,u)] \quad (3)$$

where $F(x,u)$ is the overall objective function consisting of individual objective functions of the form $F_i(x,u)$.

MO functions are solved by converting all objectives into a single objective (SO) function or by using Pareto optimization method. Conversion of the MO into a SO function is usually done by aggregating all objectives in a weighted function, or simply transforming all but one of the objectives into constraints. In this research, the former was adopted. The SO weighted function takes the form (4) [26]:

$$F(x,u) = \omega_1[F_1(x,u)] + \omega_2[F_2(x,u)] + \cdots \omega_i[F_i(x,u)] \quad (4)$$

where ω represents the weight factors of individual objective functions.

– Objective 1: operation cost minimization

Here, the objective function was mathematically formulated as minimization of aggregate operating cost consisting of power generation cost, and upregulation cost due to SPV deloading as expressed in (5) [12],

$$Minimize,$$
$$Aggregate\ Operating\ Cost = Power\ generation\ cost + Upregulation\ cost \quad (5)$$

where the *power generation cost* constitutes generation cost of thermal units and SPV power plants while the *upregulation cost* is the cost incurred for the reserve capacity for SPVPPs operating in deloaded mode. The cost function (in \$/h) is expressed as (6):

$$f = \sum_{i=1}^{ng}\left(a_i + b_i P_{gi} + c_i P_{gi}^2\right) + C_{PV} \times P_{PV} + C_{ur} \times P_{dl} \quad (6)$$

where, a_i, b_i and c_i represent SGs cost coefficients for the i^{th} generator while *ng* is the number of generators. P_{gi} - Active power output of the i^{th} generator, P_{PV} - SPV output power. C_{PV} - unit cost of SPV generation, C_{ur} - unit cost of upregulation and P_{dl} -reserve capacity for deloaded SPVPP. In this work, the SG constants used were; a=0.1 \$/h, b=0.3 \$/MWh and c=0.2 \$/MW^{2}h. For SPV, C_{PV}=61.8 \$/MWh and C_{ur}=11 \$/MWh as in [12]. SPV output power, P_{PV} and deloaded margin, P_{dl} can be written as (7) and (8):

$$P_{PV} = P_G \times pen \times \left(1 - \frac{d}{100}\right) \quad (7)$$

$$P_{dl} = P_G \times pen \times \frac{d}{100} \quad (8)$$

where *pen* represents SPVPP penetration level and *d* represents the deloading level given by (9) and (10) respectively [23]:

$$pen = \frac{PV\ output\ at\ MPPT}{Total\ power\ generated\ by\ the\ grid} \quad (9)$$

$$d = \frac{P_{dl}}{P_G \times pen} \times 100 = \frac{P_{dl}}{P_{PV} + P_{dl}} \times 100 \quad (10)$$

where P_G- aggregate power produced by all committed generators. The 1st objective function- F_C was formulated as in (11):

$$Minimize, F_c = i = 1ng\left(a_i + b_i P_{gi} + c_i P_{gi}^2\right) + C_{PV} \times P_G \times pen \times \left(1 - \frac{d}{100}\right) + C_{ur} \times P_G \times pen \times \frac{d}{100} \quad (11)$$

– Objective 2: ecological emissions reduction

In the wake of escalating climate change impacts due to GHG emissions, there is need to minimize emissions from fossil fuel thermal power plants. The carbon credit market framework has incentivized power utility companies to minimize GHG emissions. In this regard, the 2nd objective function-F_e to minimize emissions from generation technologies (in \$/h) was formulated as presented in (12) [27]:

$$F_e = \sum_{i=1}^{ng} \gamma_i P_{Gi}^2 + \beta_i P_{Gi} + \alpha_i + \zeta_i exp(\lambda_i P_{Gi}) \times C_{tax} \quad (12)$$

where C_{tax} represents the carbon tax (in \$/t). γ_i, β_i, α_i, ζ_i, and λ_i represent emission coefficients for the i^{th} generator.

– Aggregate objective function

The overall objective function-F_T was formulated by combining the $1^{st}$and 2^{nd} objective functions using appropriate weight factors (ω). It was articulated in the format prescribed by (13). In this work ω=0.5.

$$Minimize,\ F_T = \omega \times F_c + [(1 - \omega) \times F_e] \quad (13)$$

– Constraints

The formulated optimization problem is strictly bounded by the following constraints. These constraints are checked during simulations by embedding them into the python script used to implement the PSO algorithm and automate tasks. Constraints are elaborated next.

Power balance: to express the equality constraint of the power system, the total active power generated must equal to the sum of total load connected and system losses as in (14):

$$\sum_{i=1}^{ng} P_{gi} + P_{PV} = P_{Load} + P_{Loss} \quad (14)$$

Deloading level (d): the reserve margin for a deloaded SPVPP determines the deloading level, d. Operating with a large reserve margin is not financially viable as it leads to huge losses for the power utility resulting from the idle capacity (curtailed power). In this regard, there is a maximum deloading level for the SPV system considered plausible denoted as d_{max} presented in (15). Where d>0.

$$d \leq d_{max} \leq 20\% \quad (15)$$

Power generation limits: active and reactive power output limit of SGs as well as SPVPPs must be adhered to. The mathematical representation for SGs is provided in (16) and (17) while that of SPVPPs in (18) and (19):

$$P_{gi}^{min} \leq P_{gi} \leq P_{gi}^{max}\ for\ i = 1, 2, \ldots \ldots n \quad (16)$$

$$Q_{gi}^{min} \leq Q_{gi} \leq Q_{gi}^{max} \; for \; i = 1, 2, \ldots \ldots n \tag{17}$$

where P_{gi}^{min} and P_{gi}^{max}represent least and maximum possible active power output for the i^{th} SG for n number of SGs. Q_{gi}^{min} and Q_{gi}^{max} represent least and maximum possible reactive power output for the i^{th} SG for n number of SGs.

$$P_{PVj}^{min} \leq P_{PVj} \leq P_{PVj}^{max} \; for \; j = 1, 2, \ldots \; k \tag{18}$$

$$Q_{PVj}^{min} \leq Q_{PVj} \leq Q_{PVj}^{max} \; for \; j = 1, 2, \ldots \; k \tag{19}$$

where P_{PVj}^{min} and P_{PVj}^{max} represent least and maximum possible active power output for the j^{th} SPVPP for k number of SPVPPs. Q_{PVj}^{min} and Q_{PVj}^{max} represent least and maximum possible reactive power output for the j^{th} SPVPP for k number of SPVPPs.

Power system frequency stability metrics: dynamic values of frequency nadir-$f_{\_nadir}$ and RoCoF are constrained within prescribed limits for dynamic simulations for frequency secure operations as given in (20) and (21) respectively.

$$f\_nadir \geq f\_\min \tag{20}$$

$$RoCoF \leq RoCoF^{max} \tag{21}$$

here $f_{\_min}$ denotes the minimum allowable frequency after a disturbance while $f_{\_nadir}$ is the minimum frequency reached during dynamic simulation. $RocoF^{max}$ represents the maximum allowable rate of change of frequency after a frequency disturbance. After a severe disturbance, RoCoF is approximated using (22):

$$RoCoF = \frac{df}{dt} = \frac{f_0}{2} \times \frac{\Delta P}{H_{sys}} \tag{22}$$

where f_0 is nominal frequency (in hertz), ΔP is amount of power mismatch (in p.u), and H_{sys} is system inertia constant after a frequency event (in seconds).

2.3. Particle swarm optimization algorithm Implementation for determining optimal deloading level

PSO is a swarm intelligence-based computational approach inspired by the social behavior of birds and fish originally developed by Kennedy and Eberhart. PSO algorithm solves an optimization problem by creating a population of moving candidate solutions (particles) around a particular search space by deploying a simple mathematical formula based on the particle's position and velocity [26]. Movement of individual particles towards a solution is refined using the local particles best known position as well as the universal best position of the swarm discovered by other particles in the search space. Iteratively, particles update their velocity (v) and position (x) based on (23) and (24) respectively.

$$v_{i+1,p} = wv_{i,p} + c_1 r_1 \left(P_{best} - x_{i,p}\right) + c_2 r_2 \left(G_{best} - x_{i,p}\right) \tag{23}$$

$$x_{i+1,p} = x_{i,p} + v_{i+1,p} \tag{24}$$

where particle is denoted by p and i- iteration. P_{best} and G_{best} represent particle local best position and universal swarm best position, respectively whereas r_1 and r_2 represent random values. c_1 and c_2 denote the acceleration constants while w represents inertia constant.

In this research the particle position determines the optimal deloading level-d of SPVPPs. The following PSO parameters were used for this research: number of particles- $n_p = 10$, maximum number of iterations- $n_i = 30$, c_1 and c_2 were 1.2 and 2.0 respectively. The steps adopted in determining the optimal deloading level-d of SPVPPs is shown in Figure 3.

First, the PSO and optimization constraint parameters are defined. For this work the limits of frequency nadir and RoCoF were 57.16 Hz and 0.5 Hz/s, respectively. The local positions and speeds of individual particles are chosen randomly. According to the PSO algorithm, the position of each particle represents the SPVPP deloading level. Secondly, in each iteration, time domain simulations are performed for various SPV penetration levels for each particle p, using a SG outage as the severe disturbance. Using the simulation dataset, frequency response metrics such as RoCoF is calculated using (22) and frequency nadir

determined. Thirdly, the constraint parameters specified in (14)-(21) are checked for compliance with the limits set. If found to be compliant, the objective function (13) is evaluated, and the value of the particle's P_{best} is updated; otherwise, it remains constant. In the fourth step, after all particles have been evaluated, G_{best} is chosen from among the updated P_{best} as the one with the lowest value of the evaluated objective function. For the next iteration, the values of particle velocity and position are updated using (23) and (24), respectively. In step five, if the values of G_{best} meet the convergence criteria, that is if the difference in value for successive iterations is less than 0.001, the optimization process is terminated, and the updated G_{best} is considered the optimal deloading level; otherwise, steps 2–5 are repeated until the maximum number of iterations is reached.

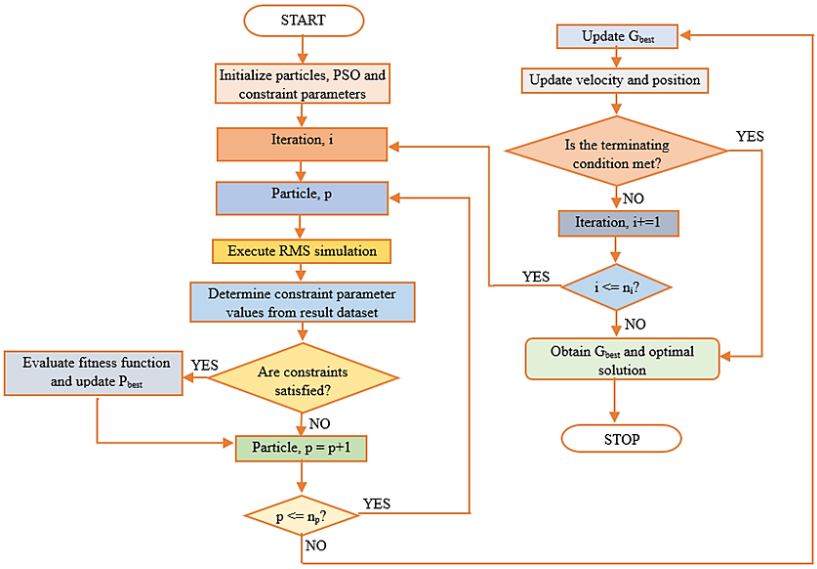

Figure 3. Flowchart for proposed optimization approach

3. CASE STUDY

3.1. Simulation setup

3.1.1. System model

Testing and validation of the dynamic model of the SPVPP in deloaded mode was done using the modified IEEE 39-bus New England System shown in Figure 4 as it has widely been used in literature to perform this role. The system was also used to investigate frequency stability analysis by carrying out dynamic simulations with integration of SPVPP. This test system has a high inertia, making it suitable for investigating frequency stability in the short-term period.

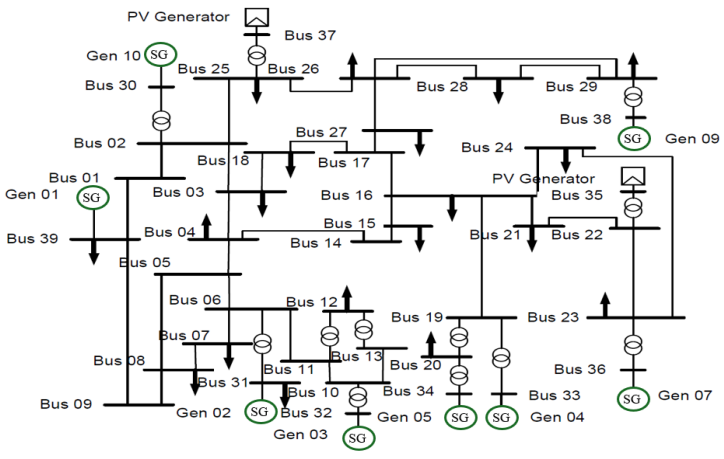

Figure 4. Single line diagram for the modified IEEE 39 bus system

Dynamic models of SGs used in the system such as governor and automatic voltage regulator are well polished standard models that have been validated by numerous previous studies fostering accuracy of dynamic simulation results [28]. The test system was therefore considered ideal for carrying out this study. The system operates at a nominal frequency of 60 Hz with a base MVA of 100. The system consists of 10 generator buses and 19 general load buses with a cumulative demand of 6.0971 GW. In a dynamic analysis of real power systems, dynamic simulation is performed only for critical events (worst case scenario). This approach is justified because analyzing all possible disturbances and operating conditions of a real power system would take an inordinate amount of time and simulations [29]. For this work, tripping of the largest and most loaded online generation unit (Gen 09) was regarded as the critical event from the frequency stability standpoint thus, representing a worst-case scenario. Two frequency stability indices were used to assess the performance of deloaded SPVPPs with FFR capability on the dynamic performance of the power system: RoCoF (df/dt) and frequency nadir. In addition, the following hourly costs were also noted; aggregated operating cost, SGs and SPV plants generation cost, ecological emission cost, and up-regulation cost.

3.1.2. Solar photovoltaic penetration

To realize different levels of SPV penetration, the SGs at buses 35, 36, and 37 were sequentially replaced with SPVPP of the same power output and rated capacity. This represented approximately 10%, 20% and 30% SPV penetration as indicated in Table 1. Variations in SPV generation due to the intermittency of solar radiation were not considered since the time domain simulation are in the very short stability time frame. In addition, for comparison purposes, a baseline scenario without SPV generation was considered. Performance of dynamic SPVPP operating in deloaded mode was also compared to static SPVPP operating at MPPT mode without FFR capability in terms of supporting frequency.

Table 1. Total system inertia constant with increasing SPV penetration

SPV penetration (%)	SPV generation (MW)	Conventional generation (MW)	Total system inertia constant-h (s)
0	0	6145.25	40.954
10	595	5550.25	37.183
20	1275	4870.25	32.833
30	1870	4275.25	29.362

3.2. Simulation results and discussion

3.2.1. Solar photovoltaic penetration without fast frequency response capability

Figure 5 shows the power system frequency response to a generator outage with increased penetration of SPV without FFR capability (static SPV). From the results in Figure 5, the scenario without SPV penetration (0% SPV pen) recorded the best performance. The power system frequency response performance deteriorated with increased adoption of static SPVPP to the grid. The frequency stability indices for each study case were determined and are summarized in Table 2.

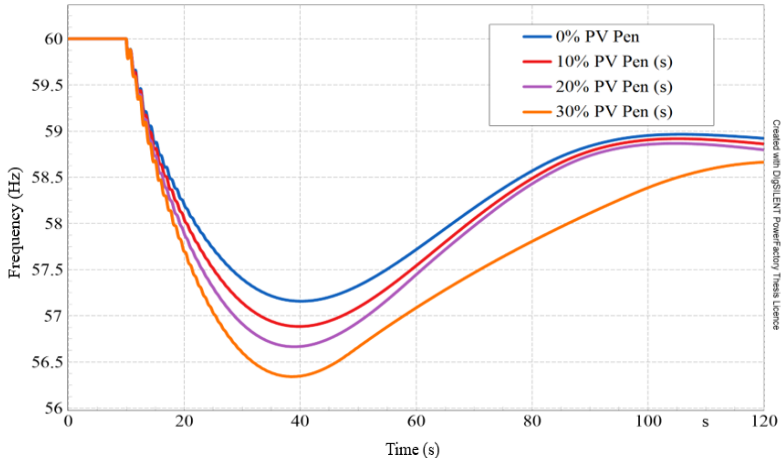

Figure 5. Frequency response with increased penetration of static SPVPPs

Table 2. Frequency stability metrics with static SPVPP penetration

Static SPV penetration level (%)	Total system inertia constant-h (s)	Frequency nadir-f_{nadir} (Hz)	RoCoF (Hz/s)
0	40.954	57.16	0.09905
10	37.183	56.88	0.1012
20	32.833	56.67	0.1193
30	29.362	56.34	0.1307

It can be observed from Table 2 that 0% SPV penetration had the highest $f_{\_nadir}$ point of 57.16 Hz and the slowest RoCoF of 0.09905 Hz/s. This better frequency response can be attributed to the presence of high levels of aggregate system average inertia provided by the rotating mass of SGs. At 30% SPV, the system records the worst frequency response performance with the lowest $f_{\_nadir}$ of 56.34 Hz and RoCoF of 0.1307 Hz/s. Increased penetration of static SPVPPs (with a constant output) reduces grid inertia which is critical in initially resisting changes in frequency after an event hence, a poor power system frequency response. Decreased inertia increases the RoCoF as provided in (22). Constant output from static SPV in case of an event worsens the frequency response as it compromises system primary frequency response with increased penetration resulting in a lower $f_{\_nadir}$ point. The results demonstrate that a power system dominated by SGs produces a better frequency response than a power system penetrated by SPVPPs.

3.2.2. Optimally deloaded solar photovoltaic penetration

The optimal deloading level (d) of SPVPPs that guarantees and preserves frequency stability of the grid was determined using PSO. The frequency response of the optimized deloaded SPVPPs was compared to the frequency response of SPVPPs supported with the inbuilt BESS frequency control model (Available in DIgSILENT PowerFactory 2023 [30]) of similar capacity as the optimal deloading level for validation purposes. The BESS model is capable of rapidly injecting active power to the grid in case of a power imbalance to arrest frequency decline.

– Study case I: 10% SPV penetration

In this study case, the optimal deloading level of the SPVPP was determined as 1.00% (5.95 MW) using PSO algorithm. PSO convergence plot is shown in Figure 6. Initially the algorithm explores the solution space characterized by a steep increase in the fitness function values where particles are actively searching for promising regions in the solution space. As iterations progress, there is a rapid decline in the fitness function. Towards latter iterations, the rate of improvement in fitness begins to significantly reduce indicating transition from exploration to exploitation phase. Here particles start converging towards better solutions. The convergence plot shows a plateau or stabilization of the fitness curve. This indicates the algorithm has reached near optimal solution or encountered convergence stagnation. At this point, further iterations may not yield significant improvements in the fitness function values.

The 1.00% deloading level resulted in a frequency response shown in Figure 7. The results are compared with the response for SPVPP and BESS frequency control. The SPVPP optimal deloading level of 1.00% produced a marginally superior frequency response compared to BESS frequency control as can be seen in Figure 7. The optimal deloading resulted in RoCoF and frequency nadir of 0.0966 Hz/s and 57.16 Hz, respectively which are within the prescribed limits whereas the corresponding values for BESS control were 0.09972 Hz/s and 57.12 Hz, respectively. The resulting optimal aggregated operating cost was $ 801,561.34 per hour.

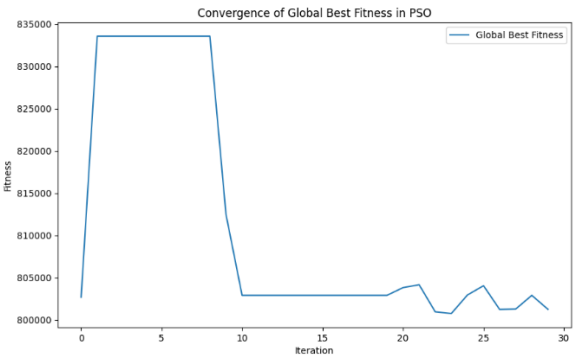

Figure 6. PSO convergence with 10% SPV penetration

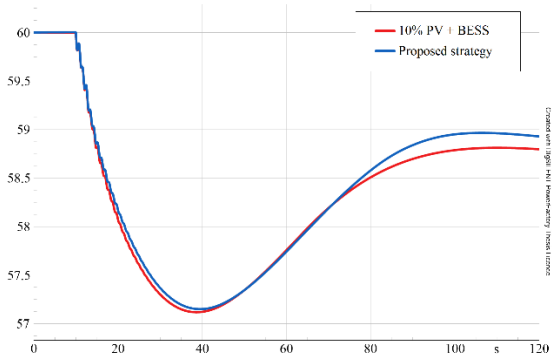

Figure 7. Frequency response of optimally deloaded SPVPP and BESS for 10% penetration

– Study case II: 20% SPV penetration

For 20% SPV penetration, the optimal deloading level was determined to be 3.43% (43.73 MW) using PSO algorithm. The PSO convergence plot shown in Figure 8. The optimization progress trend resembles the one described in study case I. An optimal deloading level of 3.43% results in a grid frequency response shown in Figure 9 with a RoCoF and $f_{\_nadir}$ of 0.09284 Hz/s and 57.32 Hz respectivelywhich meet the allowable limits of frequency stability indices. The deloaded SPV operation still provided a superior performance compared to the BESS which recorded a RoCoF and $f_{\_nadir}$ of 0.09863 Hz/s and 57.16 Hz respectively.

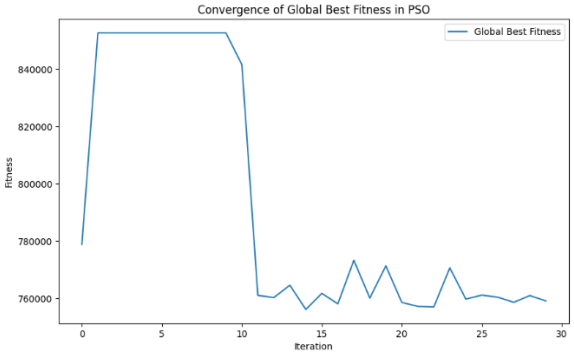

Figure 8. PSO convergence with 20% SPV penetration

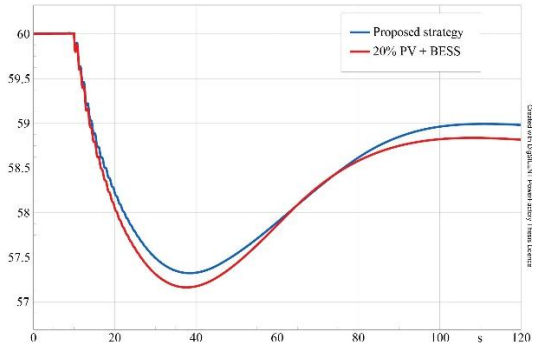

Figure 9. Frequency response of optimally deloaded SPVPP and BESS for 20% penetration

– Study case III: 30% SPV penetration

For this study case, the optimal deloading level of the SPVPPs was determined as 4.79% using PSO algorithm. The PSO convergence plot of aggregate operation cost is shown in Figure 10. The faster convergence can be attributed to the reduced search space due to tighter frequency stability constraints with decreased inertia making it easier for particles to find the optimum. The results of the dynamic simulation with optimal SPV deloading level produces a $f_{\_nadir}$ point and RoCoF of 57.40 Hz and 0.1112 Hz/s respectively as shown in Figure 11. With a minimum deloading level of 4.79%, the grid can retain the frequence response within acceptable limits ensuring that SPVPP output from the three plants is maximumly utilized to meet load demand with little power curtailment as possible for frequency response. This performance is validated by using BESS which results in a RoCoF and $f_{\_nadir}$ of 0.1211 Hz/s and 57.08 Hz respectively.

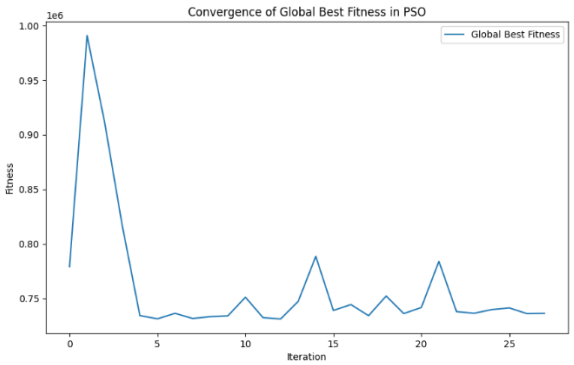

Figure 10. PSO convergence with 30% SPV penetration

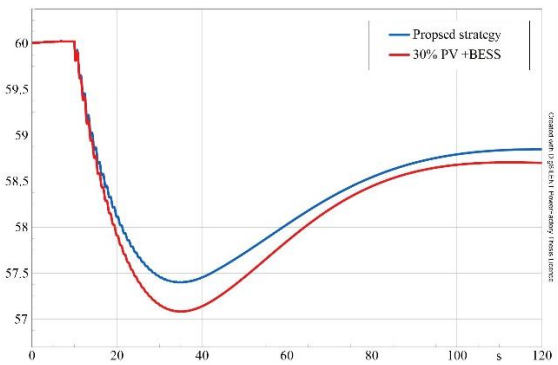

Figure 11. Frequency response of optimally deloaded SPVPP and BESS for 30% penetration

– Summarized results

Table 3 gives a summary of simulation results for optimal deloading level of SPVPPs and their respective frequency stability indices for different SPV penetration scenarios. Results in Table 3 clearly

depicts improvement in power system frequency response with optimally deloaded SPVPPs compared with BESS control for all the three SPV penetration levels. The RoCoF results show an improvement of between 3.1% for 10% penetration to 8.2% for 30% penetration when compared to BESS performance. The improvement in frequency nadir is less than 1% for all penetration levels.

Table 3. Optimal deloading level and capacity for different SPV penetration levels

SPV penetration level (%)	Optimal deloading level (%)	Deloaded capacity (MW)	Deloaded SPV generation (MW)	SG generation (MW)	Deloaded SPV RoCoF (Hz/s)	Deloaded SPV F_{nadir} (Hz)	BESS RoCoF (Hz/s)	BESS F_{nadir} (Hz)	RoCoF % age change	Fnadir % age change
10	1.00	5.95	589.4	5,561.52	0.0966	57.16	0.09972	57.12	3.1	0.1
20	3.43	43.73	1,231.27	4,917.1	0.09284	57.32	0.09863	57.16	5.9	0.3
30	4.79	89.57	1,780.28	4,377.8	0.1112	57.40	0.1211	57.08	8.2	0.6

Increasing the penetration of deloaded SPV above 10% results in better frequency response performance. This can be attributed to the ability of deloaded SPVPPs to rapidly ramp up active power held as hot reserve to settle power imbalances caused by the generator outage. The active power response is incredibly faster when using deloaded SPVPPs as compared to SGs due to the agility of power electronic converters. The FFR capability of deloaded SPVPPs is fast enough to act partly in the inertial response phase hence reduce RoCoF and can be sustained for longer periods than SG's inertial response which lasts a few seconds. According to the results in Table 3, a larger deloaded capacity of SPVPPs (89.57 MW) also ensures a higher $f_{\_nadir}$ point of 57.40 Hz. Frequency nadir is point is determined by how fast generators can increase their output to meet the power imbalance in which case the deloaded SPVPP offers superior performance. SG's delayed response due to the lethargic electromechanical response of the governor. The FFR action of deloaded SPVPPs provides an avenue for power system operators to increase their penetration levels without worrying about the average inertia levels in the power system. The results show that for FFR from deloaded SPVPPs to be effective in supporting frequency control, it must be faster in response, larger in magnitude, and sustained for an extended period.

Table 4 shows the economic benefits (reduction in aggregate operating cost) of increasing penetration of optimized deloaded SPVPPs. The aggregated optimal operating cost per hour decreased by 8.5% when the SPV penetration increased from 10% to 30%. The overall cost reduction is attributed to economic benefits of increased generation from PV which has no ecological emissions cost.

Table 4. Summary of costs associated with optimally deloaded SPVPPs for different penetration levels

SPV penetration level (%)	Aggregated operating cost ($/h)	Generation cost of SG ($/h)	Generation cost of SPV ($/h)	Ecological emission cost ($/h)	Up-regulation cost ($/h)
10	801,561.34	761,070.96	36,402.61	3,458.14	65.57
20	757,370.52	677,501.03	76,092.41	3,102.61	481.04
30	736,290.38	619,164.19	110,019.40	2,840.61	987.26

4. CONCLUSION

This paper presents a strategy for determining the optimal deloading level of SPVPPs participating in power system frequency control using PSO algorithm in DIgSILENT PowerFactory. The main contributions include formulating of a climate conscious fitness function with economic and technical considerations that can be solved using PSO algorithm to determine the optimal deloading level of SPVPPs. To better support frequency response, the FFR action from SPVPPs needed to be faster, bigger with possibility of being sustained for longer period. The research established that deloaded SPVPPs with frequency response capability can effectively and sufficiently rescue frequency decline in case of a disturbance. Considering 10%, 20% and 30% SPV penetration levels on the IEEE 39 bus test system, the optimal deloading levels were determined to be 1.00%, 3.43%, and 4.49%, respectively. Optimization of the deloading level ensures that only the FFR reserve capacity needed for frequency response is kept preventing unwarranted power curtailment from SPVPPs and reducing the aggregate operation cost of power generation. Optimal deloading of SPVPPs provides an avenue of enriching power grids with SPVPPs without worrying about decreasing levels of grid inertia. Future work will investigate whether hybrid algorithms can significantly improve optimization results. Furthermore, the proposed strategy will be applied to a real-world test system to validate the model under practical conditions such as variations in load demand and explore its effectiveness and scalability in real-world scenarios.

ACKNOWLEDGEMENT

This work was supported by Jomo Kenyatta University of Agriculture and Technology (JKUAT) through a research grant offered by Africa Development Bank (AfDB) meant for public sector capacity building in Kenya- grant number MHEST/HEST/3/61/Vol.VI.

REFERENCES

[1] B. K. Wamukoya, C. M. Muriithi, and K. K. Kaberere, "Improving frequency regulation for future low inertia power grids: a review," *Bulletin of Electrical Engineering and Informatics*, vol. 13, no. 1, pp. 76–87, Feb. 2024, doi: 10.11591/eei.v13i1.5873.

[2] C. Syranidou, J. Linssen, D. Stolten, and M. Robinius, "Integration of large-scale variable renewable energy sources into the future european power system: On the curtailment challenge," *Energies*, vol. 13, no. 20, pp. 1–23, Oct. 2020, doi: 10.3390/en13205490.

[3] A. Fernández-Guillamón, E. Gómez-Lázaro, E. Muljadi, and Á. Molina-García, "Power systems with high renewable energy sources: A review of inertia and frequency control strategies over time," *Renewable and Sustainable Energy Reviews*, vol. 115, pp. 1–12, Nov. 2019, doi: 10.1016/j.rser.2019.109369.

[4] B. K. Poolla, D. Groß, and F. Dörfler, "Placement and implementation of grid-forming and grid-following virtual inertia and fast frequency response," *IEEE Transactions on Power Systems*, vol. 34, no. 4, pp. 3035–3046, Jul. 2019, doi: 10.1109/TPWRS.2019.2892290.

[5] K. S. El-Bidairi, H. D. Nguyen, T. S. Mahmoud, S. D. G. Jayasinghe, and J. M. Guerrero, "Optimal sizing of battery energy storage systems for dynamic frequency control in an islanded microgrid: a case study of Flinders Island, Australia," *Energy*, vol. 195, pp. 1–25, Mar. 2020, doi: 10.1016/j.energy.2020.117059.

[6] Q. Hong *et al*., "Fast frequency response for effective frequency control in power systems with low inertia," *The Journal of Engineering*, vol. 2019, no. 16, pp. 1696–1702, Mar. 2019, doi: 10.1049/joe.2018.8599.

[7] V. Mallemaci, F. Mandrile, S. Rubino, A. Mazza, E. Carpaneto, and R. Bojoi, "A comprehensive comparison of virtual synchronous generators with focus on virtual inertia and frequency regulation," *Electric Power Systems Research*, vol. 201, pp. 1–13, Dec. 2021, doi: 10.1016/j.epsr.2021.107516.

[8] S. C. Johnson, D. J. Papageorgiou, D. S. Mallapragada, T. A. Deetjen, J. D. Rhodes, and M. E. Webber, "Evaluating rotational inertia as a component of grid reliability with high penetrations of variable renewable energy," *Energy*, vol. 180, pp. 258–271, Aug. 2019, doi: 10.1016/j.energy.2019.04.216.

[9] N. Nguyen, D. Pandit, R. Quigley, and J. Mitra, "Frequency response in the presence of renewable generation: challenges and opportunities," *IEEE Open Access Journal of Power and Energy*, vol. 8, pp. 543–556, 2021, doi: 10.1109/OAJPE.2021.3118393.

[10] H. Karbouj, Z. H. Rather, D. Flynn, and H. W. Qazi, "Non-synchronous fast frequency reserves in renewable energy integrated power systems: a critical review," *International Journal of Electrical Power and Energy Systems*, vol. 106, pp. 488–501, Mar. 2019, doi: 10.1016/j.ijepes.2018.09.046.

[11] A. Jawad and N. Al Masood, "A systematic approach to estimate the frequency support from large-scale PV plants in a renewable integrated grid," *Energy Reports*, vol. 8, pp. 940–954, Nov. 2022, doi: 10.1016/j.egyr.2021.12.017.

[12] I. Mahmud, N. Al Masood, and A. Jawad, "Optimal deloading of PV power plants for frequency control: a techno-economic assessment," *Electric Power Systems Research*, vol. 221, Aug. 2023, doi: 10.1016/j.epsr.2023.109457.

[13] G. Magdy, A. Bakeer, M. Nour, and E. Petlenkov, "A new virtual synchronous generator design based on the smes system for frequency stability of low-inertia power grids," *Energies*, vol. 13, no. 21, pp. 1–17, Oct. 2020, doi: 10.3390/en13215641.

[14] U. Markovic, V. Haberle, D. Shchetinin, G. Hug, D. Callaway, and E. Vrettos, "Optimal sizing and tuning of storage capacity for fast frequency control in low-inertia systems," in *SEST 2019 - 2nd International Conference on Smart Energy Systems and Technologies*, IEEE, Sep. 2019, pp. 1–6. doi: 10.1109/SEST.2019.8849022.

[15] X. Wang and M. Yue, "Design of energy storage system to improve inertial response for large scale PV generation," in *IEEE Power and Energy Society General Meeting*, IEEE, Jul. 2016, pp. 1–5. doi: 10.1109/PESGM.2016.7741690.

[16] F. Teng and G. Strbac, "Assessment of the role and value of frequency response support from wind plants," *IEEE Transactions on Sustainable Energy*, vol. 7, no. 2, pp. 586–595, Apr. 2016, doi: 10.1109/TSTE.2015.2505085.

[17] W. Yan, X. Wang, W. Gao, and V. Gevorgian, "Electro-mechanical modeling of wind turbine and energy storage systems with enhanced inertial response," *Journal of Modern Power Systems and Clean Energy*, vol. 8, no. 5, pp. 820–830, 2020, doi: 10.35833/MPCE.2020.000272.

[18] P. González-Inostroza, C. Rahmann, R. Álvarez, J. Haas, W. Nowak, and C. Rehtanz, "The role of fast frequency response of energy storage systems and renewables for ensuring frequency stability in future low-inertia power systems," *Sustainability (Switzerland)*, vol. 13, no. 10, pp. 1–16, May 2021, doi: 10.3390/su13105656.

[19] C. Zhang, E. Rakhshani, N. Veerakumar, J. L. R. Torres, and P. Palensky, "Modeling and optimal tuning of hybrid ESS supporting fast active power regulation of fully decoupled wind power generators," *IEEE Access*, vol. 9, pp. 46409–46421, 2021, doi: 10.1109/ACCESS.2021.3066134.

[20] R. Eriksson, N. Modig, and K. Elkington, "Synthetic inertia versus fast frequency response: a definition," *IET Renewable Power Generation*, vol. 12, no. 5, pp. 507–514, Apr. 2018, doi: 10.1049/iet-rpg.2017.0370.

[21] P. Perumal, A. K. Ramasamy, and A. M. Teng, "Performance analysis of the DigSILENT PV model connected to a modelled malaysian distribution network," *International Journal of Control and Automation*, vol. 9, no. 12, pp. 75–88, 2016, doi: 10.14257/ijca.2016.9.12.07.

[22] T. U. Badrudeen, N. I. Nwulu, and S. L. Gbadamosi, "Low-inertia control of a large-scale renewable energy penetration in power grids: A systematic review with taxonomy and bibliometric analysis," *Energy Strategy Reviews*, vol. 52, pp. 1–15, Mar. 2024, doi: 10.1016/j.esr.2024.101337.

[23] C. Rahmann and A. Castillo, "Fast frequency response capability of photovoltaic power plants: the necessity of new grid requirements and definitions," *Energies*, vol. 7, no. 10, pp. 6306–6322, Sep. 2014, doi: 10.3390/en7106306.

[24] R. Rajan, F. M. Fernandez, and Y. Yang, "Primary frequency control techniques for large-scale PV-integrated power systems: a review," *Renewable and Sustainable Energy Reviews*, vol. 144, pp. 1–18, Jul. 2021, doi: 10.1016/j.rser.2021.110998.

[25] P. P. Zarina, S. Mishra, and P. C. Sekhar, "Exploring frequency control capability of a PV system in a hybrid PV-rotating machine-without storage system," *International Journal of Electrical Power and Energy Systems*, vol. 60, pp. 258–267, Sep. 2014, doi: 10.1016/j.ijepes.2014.02.033.

[26] A. G. Gad, "Particle swarm optimization algorithm and its applications: a systematic review," *Archives of Computational Methods in Engineering*, vol. 29, no. 5, pp. 2531–2561, Aug. 2022, doi: 10.1007/s11831-021-09694-4.

[27] S. Albatran, S. Harasis, M. Ialomoush, Y. Alsmadi, and M. Awawdeh, "Realistic optimal power flow of a wind-connected power system with enhanced wind speed model," *IEEE Access*, vol. 8, pp. 176973–176985, 2020, doi: 10.1109/ACCESS.2020.3027065.
[28] P. Demetriou, M. Asprou, J. Quiros-Tortos, and E. Kyriakides, "Dynamic IEEE test systems for transient analysis," *IEEE Systems Journal*, vol. 11, no. 4, pp. 2108–2117, Dec. 2015, doi: 10.1109/jsyst.2015.2444893.
[29] A. Cabrera-Tobar, E. Bullich-Massagué, M. Aragüés-Peñalba, and O. Gomis-Bellmunt, "Review of advanced grid requirements for the integration of large scale photovoltaic power plants in the transmission system," *Renewable and Sustainable Energy Reviews*, vol. 62, pp. 971–987, Sep. 2016, doi: 10.1016/j.rser.2016.05.044.
[30] DIgSILENT, "Technical Reference DIgSILENT battery energy storage system template DIgSILENT BESS FrequencyCtrl 10kV 30MVA." [Online]. Available: https://www.digsilent.de. (Accessed: Feb. 11, 2024).

BIOGRAPHIES OF AUTHORS

Brian K. Wamukoya holds a B.Sc. Degree in Electrical and Electronic Engineering (2015) from Jomo Kenyatta University of Agriculture and Technology (Kenya) and a Master's Degree in Energy Engineering (2018) from Pan African University Institute of Water and Energy Sciences (PAUWES), Tlemcen, Algeria, and is currently pursuing a Ph.D. in Electrical Engineering at JKUAT. He is a registered Professional Engineer with the Engineers' Board of Kenya (EBK). He has eight years of experience cutting across industry, teaching, and research. His research interests are power system modeling and optimization, renewable energy systems and grid integration. He can be contacted at email: wamukoya.brian@students.jkuat.ac.ke.

Keren K. Kaberere received her B.Sc. Degree in Electrical and Electronic Engineering (1993), M.Sc. in Electrical Engineering (1999) from University of Nairobi (Kenya), and Ph.D. Degree (2006) in Electrical Engineering from University of Cape Town (UCT) in South Africa. She is currently a Senior Lecturer with the Department of Electrical and Electronic Engineering, JKUAT and an energy consultant. Her research interests include power system modelling and stability, power economics, energy management, and energy policy formulation. She can be contacted at email: kkanuthu@eng.jkuat.ac.ke.

Christopher M. Muriithi received B.Eng. Degree and M.Eng. in Electrical Engineering from Mosco Power Engineering Institute (Technical University), Russia, in 2001 and 2003 respectively. He was awarded a Ph.D. in Electrical Engineering from JKUAT in 2012. He is currently a Professor with the Department of Electrical and Electronic Engineering, Murang'a University of Technology, Kenya. He is a registered Professional Engineer with the Engineers' Board of Kenya (EBK). His research interests include Power system modelling, renewable energy integration, power system state estimation and control, and electrical machines. He can be contacted at email: cmmuriithi@mut.ac.ke.